Atomic and Electronic Structure at Au/CdSe Interfaces

R. de Paiva and Rosa Di Felice*

National Center on nanoStructures and bioSystems at Surfaces (S3) of INFM-CNR, Via Campi 213/A, 41100 Modena, Italy

ABSTRACT By means of plane-wave pseudopotential periodic-supercell density functional theory calculations with a gradient-corrected exchange-correlation functional, we investigated the formation and the electronic structure of thin Au overlayers on CdSe(0001) and CdSe(000$\bar{1}$) surfaces. We explored several possible Au/CdSe interfaces, including nonstoichiometric cases in which the very interface layer is mixed, namely, contains atoms of both the metal and the semiconductor. The relative formation energies of the computed model structures indicate that the formation of a very thin Au layer on CdSe surfaces can be epitaxial in the very early deposition stages but only in rather Au-rich conditions. The analysis of the band structures, densities of states, and wave functions for the low-energy interfaces reveals that hybridization occurs between the metal and the semiconductor electron states. This hybridization is confined at the very interface and is not expected to have significant consequences on the plasmonic and excitonic excitations that are appealing for nanotechnology applications of metal−semiconductor nanoparticles.

KEYWORDS: Au/CdSe hybrid interfaces · density functional theory · electronic structure · stability · interface electronic mixing

Hybrid metal−semiconductor nanoparticles have attracted great interest due to their potential application in developing future electronic and optoelectronic nanodevices. The possibility to design the functionalities by tailoring shape and size, as well as to exploit the combination of properties from the semiconductor (electrical or optical) and from the metal (optical, electrical, chemical, connectivity), suggests many viable devices, including ultrasmall transistors, memory elements, light-emitting elements, and sensors.[1,2] Despite this huge potential, most applications of nanoparticles have been limited so far to isotropic shapes, and metal−semiconductor nanohybrids have been little investigated. These limitations were especially due to difficulties in their production.

Recently, successful synthesis paradigms for semiconductor rods (mostly CdSe) and successively for Au/CdSe and Au/CdS nanodumbbells have been demonstrated.[3−6] These experimental achievements have significantly driven efforts to characterize their optical and electrical performance, as well as to theoretically understand their properties.[7−15] Besides the potential applications, the electronic properties of semiconductor nanorods and hybrid metal−semiconductor nanodumbbells are extremely interesting from a fundamental viewpoint, to investigate the mixing of electron states between two different materials in a size regime where quantization effects are expected to play a major role.

In this context, we have carried out a plane-wave pseudopotential density functional theory study of Au thin films on CdSe(0001) and CdSe(000$\bar{1}$) surfaces, with the aim to understand if atomic mixing between atoms of the overlayer and of the substrate occurs, how it is affected by different chemical environments, and what are the consequences of the mixing on the bandstructure of the hybrid system. This is a first required step to unravel metastable interface geometries and mechanisms for electronic mixing that may occur also in confined nanoparticles. We remark that, while the reconstructions of CdSe(0001) and CdSe(000$\bar{1}$) surfaces have already been tackled with *ab initio* methods in the context of understanding the structural properties of CdSe nanorods, the Au/CdSe interfaces that are relevant in hybrid nanodumbbells have not yet been explored so far by any computational approach.[9−11,14,15] We have considered several possible geometries for strained gold thin layers on the two CdSe polar surfaces, allowing for stoichiometric and nonstoichiometric interface layers. We present stability diagrams, densities of states, and electron wave functions. The analysis of the results reveals that stable Au bilayers may be formed on CdSe surfaces within the

*Address correspondence to rosa.difelice@unimore.it.

Received for review July 22, 2008 and accepted October 27, 2008.

Published online November 25, 2008.
10.1021/nn8004608 CCC: $40.75

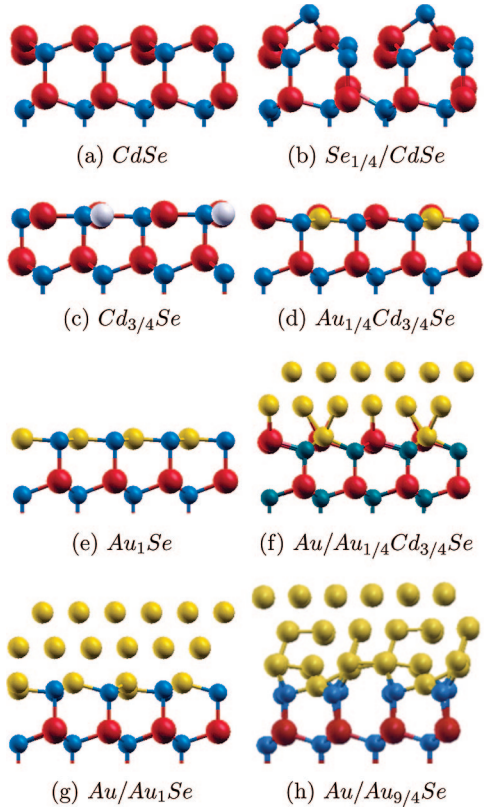

Figure 1. Side view of relaxed atomic structures for all the configurations that we examined to model the CdSe(0001) surface and the Au/CdSe(0001) interface. Red, blue, and yellow spheres represent Cd, Se, and Au atoms, respectively. White spheres in panel (c) represent Cd vacancies.

allowed range of Cd chemical potential and in Au-rich conditions. Significant orbital mixing between Se and Au occurs at the interface. Although current growth methods likely do not produce epitaxial structures, we believe that our results may, on one hand, give indications on how to stabilize very thin ordered layers that fix the kind of interface mixing and, on the other hand, are anyway representative of qualitative features that occur upon metal−semiconductor electronic interaction.

RESULTS AND DISCUSSION

CdSe(0001) and Au/CdSe(0001): Structure and Energetics. The equilibrium atomic geometries obtained after relaxing the CdSe(0001) surfaces and the Au/CdSe(0001) interfaces are shown in Figure 1. The rationale for their choice is explained in the final section devoted to the methodologies.

To model the clean surfaces, we took into account previous DFT results that pointed out the Cd vacancy ($Cd_{3/4}Se$) (Figure 1c) and the Se adatom ($Se_{1/4}/CdSe$) 2 × 2 (Figure 1b) structures as the lowest energy ones among several other possibilities.[9,14,15] We also took into account as a starting condition the bulk-terminated 1 × 1 (0001) face CdSe: in the computational 2 × 2 supercell, it relaxes toward a less symmetric pseudo 1 × 1 geometry shown in Figures 1a and 2a. The Au thin

TABLE 1. Calculated Vertical Atomic Displacements (in Å) at the Three Outermost Bilayers of Cd- and Au-Terminated CdSe(0001), Relative to the Bulk-like Positions. Positive (Negative) Values Indicate Outward (Inward) Displacements

bilayer	atom	CdSe	$Cd_{3/4}Se$	$Se_{1/4}/CdSe$	$Au_{1/4}Cd_{3/4}Se$	Au_1Se
1_{Cd}	Cd*/Au*	−0.77		−0.98	−0.50 (Au)	
	$\overline{Cd}/\overline{Au}$	0.05	−0.69	0.15	−0.36	−0.55 (Au)
1_{Se}	Se*		0.07	0.53		
	$\overline{Se}$	0.04	0.17	−0.26	0.14	0.20
2_{Cd}	Cd*		0.01	0.48	0.00	
	$\overline{Cd}$	0.00	0.15	−0.25	0.07	0.13
2_{Se}	Se*			−0.19		0.20
	$\overline{Se}$	0.04	0.04	0.01	0.06	0.07
3_{Cd}	Cd*			−0.17		
	$\overline{Cd}$	0.01	0.03	0.01	0.03	0.06
3_{Se}	$\overline{Se}$	−0.01	0.00	−0.02	0.03	0.03

films were obtained gradually by subsequent steps: (1) filling the top Cd vacancies with Au atoms, yielding the $Au_{1/4}Cd_{3/4}Se$ structure of Figure 1d; (2) replacing the whole top 2 × 2 Cd layer with a 2 × 2 Au layer, which is under substantial tensile strain, structure Au_1Se in Figure 1e; (3) adding a full 3 × 3 Au(111) bilayer on top of the surface of Figure 1d (structure $Au/Au_{1/4}Cd_{3/4}Se$ in Figure 1f); (4) adding a full 3 × 3 Au(111) bilayer on top of the surface of Figure 1e (structure Au/Au_1Se in Figure 1g); (5) replacing the strained 2 × 2 Au interface layer of Figure 1g with a 3 × 3 Au layer while imposing the correct fcc (111) stacking through the Au thickness (structure $Au/Au_{9/4}Se$ in Figure 1h).

In Table 1, we report the vertical atomic displacements in the three topmost bilayers of the supercell, for the bare Cd-terminated surfaces and for the Au-terminated surfaces in which the top Cd layer is partially or totally substituted with Au atoms. Each neutral bilayer is constituted of a Se plane and a Cd plane separated by $c/8$, whereas two contiguous bilayers are separated by the larger distance of $3c/8$, where c is the bulk lattice constant perpendicular to the hexagonal (0001) plane. $\overline{Cd}(\overline{Se})$ denotes the average of equivalent Cd (Se) atoms in a given layer. Cd*(Se*) denotes one out of four atoms in a plane, which behaves differently, or the Se adatom. Some other structural details are reported for the pure CdSe(0001) surfaces in Figure 2.

Large inward displacements are found in the top plane in all the tabulated geometries. Such displacements are connected to the need for lowering the total energy by adjusting the charge in the surface dangling bonds.

In the pseudo 1 × 1 CdSe structure, we find that one of the four surface cations (restatom, Cd* in Table 1) moves inward by 0.77 Å and the other three cations remain almost at the ideal height (0.05 Å outward), as well as the Se atoms in the same bilayer. This can be associated to a charge transfer from the Cd restatom to the other Cd atoms, so that it empties its dangling bond, satisfying for itself the electron counting rule.

The other dangling bonds remain partially filled (2 electrons shared among 3 atoms), and the surface is metallic. This mechanism does not lead to an energetically favorable structure, as we see below with the discussion of the energetics, because the electron counting rule is not globally satisfied. The Cd−Se distance at the first bilayer is contracted by 0.11 Å relative to the bulk bond length for the Cd restatom, whereas the variation is negligible for the other bond lengths in the same bilayer.

In the $Cd_{3/4}Se$ structure, all the cations in the surface plane move inward by 0.69 Å, so that the top bilayer is almost flat in a sp^2-like coordination (Figure 1c). This movement is associated with a charge transfer of 1/2 electron from each of the three top Cd atoms to fill the Se dangling bonds that remain upon creation of the Cd vacancy: the Se dangling bonds contain 6/4 of an electron each, so they are completely saturated by such a charge transfer. As a consequence, these Se atoms move outward by 0.17 Å. This mechanism produces a low-energy surface with a semiconducting behavior. All the cation dangling bonds are empty, and all the anion dangling bonds are full, thus perfectly satisfying the electron counting rule. The energetics indeed shows that this is the lowest energy structure for the clean CdSe(0001) surface, with no surface states in the electronic band gap. The Cd−Se distances in the first bilayer remain practically equal to the bulk bond length.

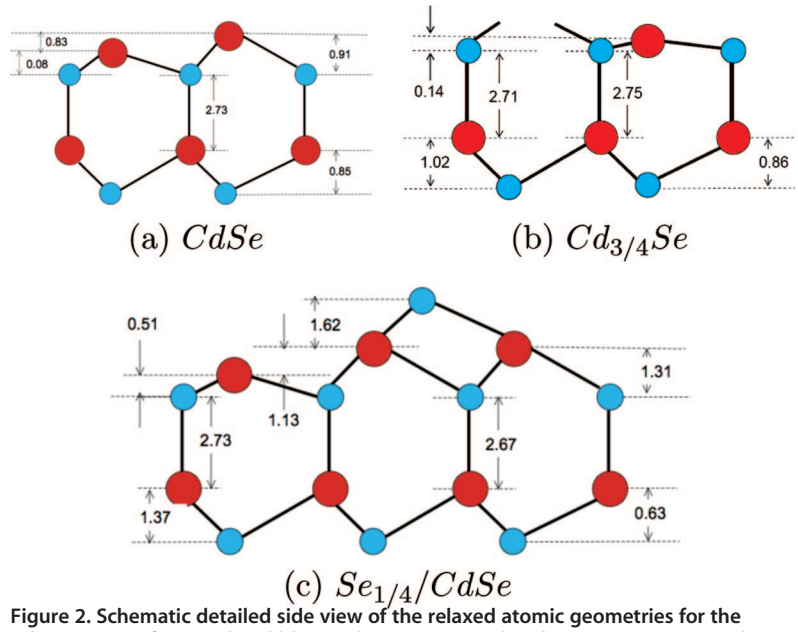

Figure 2. Schematic detailed side view of the relaxed atomic geometries for the CdSe(0001) surface. Red and blue circles represent Cd and Se atoms, respectively.

In the $Se_{1/4}$/CdSe structure, the three Cd atoms coordinated to the Se adatom move outward by 0.15 Å, while the remaining Cd restatom (Cd* in Table 1) moves inward by 0.98 Å. The three selenium atoms coordinated to the Cd restatom move inward by 0.26 Å toward an almost sp^2-like bonding, whereas the fourth Se atom in the first bilayer moves outward by 0.53 Å to adjust the charge redistribution. The Se adatom is located 1.62 Å above the plane of its three Cd neighbors with corresponding Cd−Se bond length of 2.64 Å, rather similar to the bulk bond length of 2.69 Å. This rearrangement is associated with a charge transfer from the Cd restatom to the Se adatom, so that the cation dangling bond is empty and the anion dangling bond is full. The mechanism again satisfies the electron counting rule and gives a low-energy structure. However, there is an occupied surface state in the electronic band gap due to the adatom dangling bond, and consequently the $Se_{1/4}$/CdSe reconstruction has a slightly higher energy than the $Cd_{3/4}Se$ reconstruction, as we show in detail below. The Cd−Se distance for the restatom is contracted by 0.14 Å relative to the bulk bond length, while it is unchanged for the other Cd atoms at the first bilayer.

As to the two gold-terminated surfaces listed in Table 1, we just point out on the first layer an overall depression toward the bulk, larger in the case when the full Cd top layer is substituted by Au.

The above displacements at the top bilayer are propagated much more mildly below the surface. In the second bilayer, we still obtain asymmetric atomic shifts due to the accommodation of the bonded atoms above. In the third bilayer, instead, the atomic displacements relative to the bulk configuration are practically negligible, even in the Au-terminated surfaces. The Cd−Se distances in the second and third bilayers are equal to the bulk bond length within 0.02 Å. The lateral displacements are negligible in all the planes.

Our results thus indicate that the surface reconstruction is essentially limited to the two outermost bilayers. This indication is in agreement with previous studies and is an indirect proof that the slab thickness adopted by us is large enough for an accurate description of the system.[9] The Au/CdSe(0001) interfaces with thicker Au overlayers, Au/$Au_{1/4}Cd_{3/4}Se$, Au/Au_1Se, and Au/$Au_{9/4}Se$, are not analyzed in detail but are in line with this finding. The Au/$Au_{1/4}Cd_{3/4}Se$ and Au/Au_1Se structures have still vertical displacements of the order of 0.1 Å at the third bilayer, but vanishing below. The Au/$Au_{9/4}Se$ structure exhibited during the relaxation an overall drift, and the displacements are not significant, but it is evident that at the third CdSe bilayer it has the correct hexagonal symmetry of the 2 × 2 lattice.

In Figure 3, we report our results about the relative energetics of the explored CdSe(0001) surfaces and Au/CdSe(0001) interfaces. The plots in Figure 3a,b report the formation energy as a function of the Cd chemical potential according to eq 2 (see Theoretical Framework) with two different fixed values of the Au chemical potential, $\mu_{Au} = \mu_{Au(bulk)}$ and $\mu_{Au} = \mu_{Au(bulk)} - 0.25$ eV in Figure 3a,b, respectively. The plot of Figure 3c reports

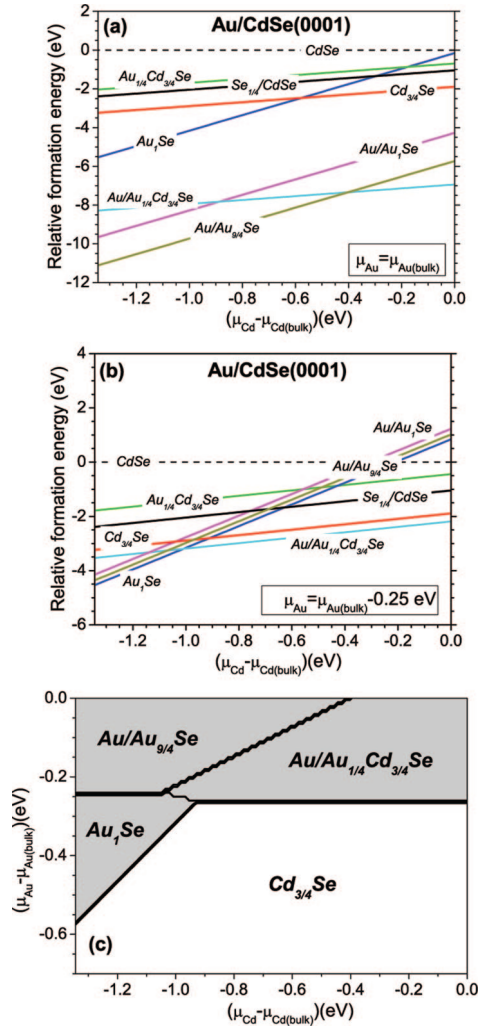

Figure 3. (a) Relative formation energy, computed with respect to the arbitrary reference pseudo 1 × 1 surface, as a function of the Cd chemical potential for a fixed Au abundance equal to that of bulk fcc Au (Au-rich conditions). (b) Relative formation energy, computed with respect to the arbitrary reference pseudo 1 × 1 surface, as a function of the Cd chemical potential for a fixed Au abundance lower than that of bulk fcc Au. (a,b) Cd-rich (Se-rich) conditions mark the upper (lower) limit of the horizontal axis. (c) Phase diagram representing the lowest energy structure in the plane of variability of both μ_{Au} and μ_{Cd}. The upper limit of μ_{Au} corresponds to Au-rich conditions, fixed at bulk fcc Au, and an arbitrary lower limit is chosen. The upper (lower) limit of μ_{Cd} corresponds to a Cd-rich (Cd-poor equivalent to Se-rich), fixed at bulk hcp Cd, CdSe surface with respect to the stoichiometric bulk: the lower limit is fixed by the formation energy of bulk CdSe (see Theoretical Framework).

the lowest energy structure for any values of the Au and Cd chemical potentials according to eq 2 (see Theoretical Framework) where both μ_{Au} and μ_{Cd} are let free to vary in a physically viable range. The evaluation of the relative energetics is explained in the methodological section.

As a general observation, we point out the positive slope of the lines for all the structures (except the flat stoichiometric CdSe), by which in Cd-rich conditions all the structures have a larger relative formation energy than in Cd-poor conditions. This behavior simply reflects the surface layout of lower Cd abundance than in the bulk because Cd atoms are removed from the top plane or Se adatoms are added in the case of $Se_{1/4}$/CdSe; hence, the surfaces are generally more stable in Cd-poor conditions.

The plot of Figure 3a shows that in extremely Au-rich conditions, equivalent to bulk gold, two of the investigated Au thin films become energetically favorable with respect to the bare CdSe surfaces. The $Au/Au_{1/4}Cd_{3/4}Se$ structure (Figure 1f) has the lowest energy in Cd-rich conditions, and the $Au/Au_{9/4}Se$ structure (Figure 1g) becomes most stable toward Cd-poor conditions, with a transition at $\mu_{Cd} = \mu_{Cd(bulk)} - 0.40$ eV. The alternation between the two geometries conforms to the rationale that in Cd-poor conditions it is easier to remove Cd atoms for substituting them with Au atoms: in fact, the $Au/Au_{9/4}Se$ interface needs more of such removal and therefore needs Cd-poor conditions to become feasible.

If the Au abundance is decreased, namely, if a lower value is fixed for μ_{Au}, as, for example, in Figure 3b, the relative formation energy of Au-covered surfaces increases relative to the bare surfaces and epitaxial gold overlayers become increasingly more and more unfavorable. For $\mu_{Au} = \mu_{Au(bulk)} - 0.25$ eV, the $Au/Au_{1/4}Cd_{3/4}Se$ structure is still favorable in Cd-rich conditions, but in Cd-poor conditions, the $Au/Au_{9/4}Se$ thin film configuration is overcome by the Au-terminated surface Au_1Se. The transition between $Au/Au_{1/4}Cd_{3/4}Se$ and Au_1Se occurs for $\mu_{Cd} = \mu_{Cd(bulk)} - 1.04$ eV. This picture still complies with the rationale that in Cd-poor conditions it is easier to remove a large number of Cd atoms and create a mixed Se−Au interface. However, it is no longer favorable to put additional Au material on top of it because of the energy cost for strain that increases with the amount of material.

By further decreasing the Au chemical potential, we find that no thin films or mixed interfaces are energetically favorable, independently of the Cd stoichiometry, for μ_{Au} below $\mu_{Au(bulk)} - 0.6$ eV. Our results indicate that it is possible to deposit very thin epitaxial Au overlayers on the CdSe(0001) surface, provided that Au-rich conditions are adopted in the preparation protocol. However, even in extremely Au-rich conditions, we expect that the strain energy at some thickness overcomes the energy gain for the accumulation of the gold atoms in the overlayer and must be released by lifting the epitaxial constraint. A detailed analysis of this phenomenon is beyond the scope of the present paper, which is instead devoted to unravel the features of electronic metal−semiconductor coupling at viable interfaces.

The results can be recast into the form of a phase diagram that features the most favorable structure in the (μ_{Cd}, μ_{Au}) plane: this is shown in Figure 3c. Such a phase diagram practically summarizes the evidence

outlined above by commenting the plots of the relative formation energy.

Among all the investigated surfaces and interfaces, only four structures play a role in the stability diagram. The bare $Cd_{3/4}Se$ surface is most favorable, independently of the Cd abundance, for any Au abundance lower than that corresponding to $\mu_{Au} = \mu_{Au(bulk)} - 0.6$ eV, namely, in all the lowest part of the stability diagram. For $\mu_{Au(bulk)} - 0.6\ eV \leq \mu_{Au} \leq \mu_{Au(bulk)} - 0.27$ eV, there is an alternation between the Au_1Se and the $Cd_{3/4}Se$ surfaces in Cd-poor and Cd-rich conditions, respectively. This means that it is possible to form a mixed interface, but no real metallic gold can be added on top. A particularly appealing condition emerges for Cd-poor/Au-rich conditions, where one can gradually form the Au_1Se mixed interface and then, by increasing the Au abundance, change the registry and stoichiometry of the very first Au layer and incorporate more fcc Au(111), thus forming the ($Au/Au_{9/4}Se$) system.

In practice, the only useful window to produce epitaxial gold thin films on top of CdSe(0001) would be that corresponding to the upper left corner of Figure 3c. Although these conditions may be harsh to realize in real synthesis protocols of hybrid nanoparticles, our study yet indicates that ordered Au films are energetically viable and suggests possible structures in which it makes sense to investigate the electronic metal−semiconductor coupling. Let us also keep into account that, even if at some point the strain must be released and the real structures are no longer epitaxial, the interface geometry may be pinned, and any of the three mixed interfaces studied by us (Figure 1f−h) is likely to represent a realistic interface electronic structure.[6]

We note that the structure Au/Au_1Se is never favorable relative to the structure $Au/Au_{9/4}Se$; this is an index that structures that immediately release the strain as much as possible in the interface layer are preferred. In fact, the 2×2 Au first layer of Au/Au_1Se is substantially strained, whereas the 3×3 corresponding plane of $Au/Au_{9/4}Se$ is much less strained and at the same time in registry with the overlying material.

CdSe(0001) and Au/CdSe(0001): Electronic Properties. In Figures 4 and 5, we plot the layer projected density of states (PDOS) and the bandstructure, respectively, for the lowest energy CdSe(0001) surfaces and Au/CdSe(0001) interfaces that appear in the stability diagram discussed in the previous subsection. The labeling convention is explained in detail in the figure captions.

Before discussing the PDOS for the surface/interface phases, let us summarize the atomic orbital projected DOS for the bulk phases of CdSe and Au, wurtzite and fcc, respectively (shaded areas in Figure 4). In wurtzite CdSe, the 4s Se and 4d Cd states are deep in the energy spectrum and have little contribution to the Cd−Se bonding. The wide bands located in the range

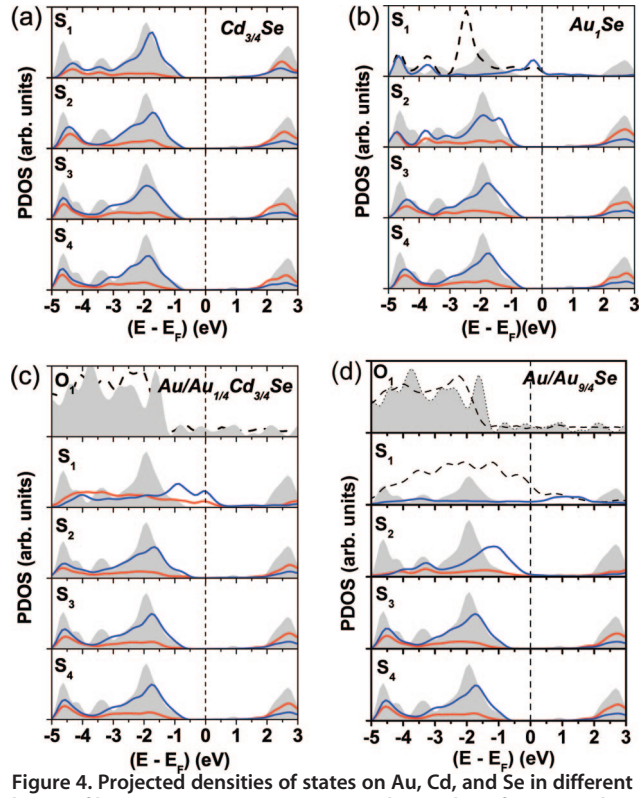

Figure 4. Projected densities of states on Au, Cd, and Se in different layers of lowest energy systems among the totality of computed structures of the Cd-terminated CdSe(0001) surface and Au/CdSe(0001) interfaces, namely, those that appear in the phase diagram of Figure 3. The labels of the structures conform to the definitions in Figure 1. S_1, S_2, S_3, and S_4 indicate the four topmost substrate bilayers; O_1 indicates the Au overlayer on top of the S_1 bilayer. The S_1 bilayer is purely CdSe in $Cd_{3/4}Se$, purely AuSe in Au_1Se and Au/Au_1Se, while the Cd layer is mixed with Au atoms in $Au/Au_{1/4}Cd_{3/4}Se$. The shaded gray area is the CdSe-wurtzite bulk DOS in the panels for substrate bilayers and is the Au fcc bulk DOS in the panels for the overlayer. The solid red and blue lines indicate the contributions of the Cd and Se states, respectively. The dashed black lines indicate the contributions of the Au states. The vertical lines denote the positions of the Fermi energy. The bottom of the valence band from interface calculations is aligned with the bottom of the valence band of wurtzite bulk CdSe. Layer S_4 is representative of the bulk features.

of −5.0 to −1.0 eV show a large hybridization between 4p Se and 5s Cd states. The top of the valence band is dominated by 4p Se states. The bottom of the conduction band consists mainly of 5s and 5p Cd states. In fcc Au, the DOS from −7.0 to −1.0 eV is due to 5d orbitals, whereas the metallic states that cross the Fermi level are mainly 6s and 6p states.

With this overview on the bulk electronic features in mind, we now turn to a discussion of the PDOS curves of Figure 4, with a special focus on highlighting if and how the above-mentioned electron states coming from the two components mix. We show and discuss only the DOS curves of structures that appear in the relative stability diagram of Figure 3c. Among the free CdSe(0001) surfaces, for instance, we focus on the $Cd_{3/4}Se$ structure. For what concerns the other two investigated structures, the relaxation/reconstruction mechanisms discussed above give origin to a metallic

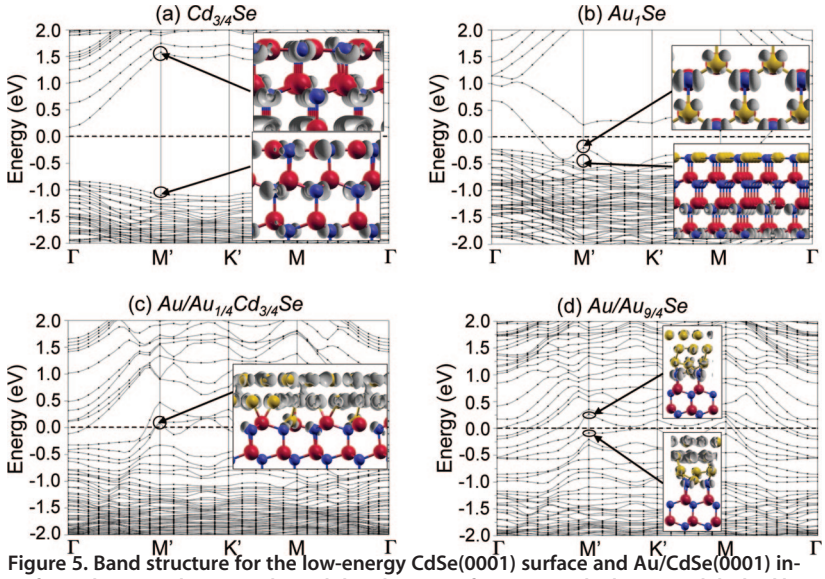

Figure 5. Band structure for the low-energy CdSe(0001) surface and Au/CdSe(0001) interfaces that are relevant in the stability diagram of Figure 3c. The horizontal dashed lines denote the positions of the Fermi level, set at the origin of the energy scale. The insets represent electron states at the M′ point around the band gap of semiconducting structures or the Fermi level of metallic structures, which were selected to highlight the dominant traits of electronic mixing and are described in the text.

pseudo 1 × 1 CdSe surface with a finite DOS at the Fermi level due to the Cd dangling bonds and to a semiconducting $Se_{1/4}$/CdSe surface with a vanishing DOS at the Fermi level and a surface band due to the occupied Se adatom dangling bond. In this semiconducting surface, the top of the occupied bands is due to Se p states, and the shape of the Se PDOS is significantly different in the topmost layer from its shape in the bulk.

At the $Cd_{3/4}Se$ surface, the inward relaxation of the Cd cations is compatible with filling the Se dangling bonds created by the Cd vacancy in each 2 × 2 cell, with the consequent formation of a semiconducting structure that has a vanishing DOS at the Fermi level. This was suggested above on the basis of the structural features and is found explicitly in Figures 4a and 5a. Figure 4a demonstrates the existence of a band gap that at the surface bilayer S_1 is equal to the bulk band gap. Also the shape of the occupied and empty PDOS on both Cd and Se remains practically the same as in the bulk. In fact, this structure has no surface states in the gap (see Figure 5a) and is very stable (Figure 3). The isosurface plots in the insets of Figure 5a show that the topmost occupied and lowest unoccupied bands are due to bulk-like Se orbitals. These very orbitals are expected to be responsible for the interaction with the metallic states of the gold overlayer when Au is grown on top of the surface.

For the Au_1Se and $Au_{1/4}Cd_{3/4}Se$ structures, the presence of Au atoms in the whole top layer or in the site created by the Cd vacancy does not change the bonding configuration of Se but modifies the nature of the electronic wave functions because of the different electronegativity of Au and Cd. These changes are concentrated on the layers next to the surface, mainly S_1 and S_2 as shown in the PDOS curves of Figure 4b. In fact, it is evident that only the Au- and Se-projected PDOSs in the top panel cross the Fermi level, namely, the metallic states are confined in the topmost bilayer S_1. In S_2, we observe a major modification with respect to the bulk shape of the Cd- and Se-projected PDOSs. At the Fermi level, both the Au- and Se-projected S_1 PDOSs are finite, indicating a possible mixing between Au and Se orbitals. This is evidenced in Figure 5b, which confirms the existence of one metallic band that crosses the Fermi level between Γ and M′. The width of this band, calculated as the energy difference between the maximum at Γ and the minimum along the ΓM′ direction, is 1.11 eV. The band is quite similar along the MΓ direction, but the minimum is at M rather than at an intermediate point, and the bandwidth is slightly larger. The shape of the orbital in the top inset (top view) illustrates that this metallic band is due to the hybridization between Au d states and Se p states. The shape of the orbital in the bottom inset (side view) illustrates that the band immediately below the metallic band is due to bulk-like states. In other words, only the Se p orbitals in the top bilayer are affected by the presence of Au.

Also the two structures with an additional Au bilayer on top of the mixed Se−Au interface, $Au/Au_{1/4}Cd_{3/4}Se$ and $Au/Au_{9/4}Se$, are metallic, as one could expect. The metallization of the interfaces increases with Au coverage, as illustrated in Figure 4c,d; the Au overlayer O_1 and the substrate bilayer S_1 have a metallic character. As in the very early Au_1Se interface described above, the Se-projected DOS crosses the Fermi level in S_1, indicating the metallization of the Se orbitals as a consequence of the presence of Au. A look at selected wave functions in Figure 5c,d demonstrates again the hybridization between Au d and Se p orbitals. The number of metallic bands increases.

CdSe (000$\bar{1}$) and Au/CdSe (000$\bar{1}$): Structure and Energetics. The equilibrium atomic geometries obtained after relaxing the CdSe(000$\bar{1}$) surfaces and the Au/CdSe(000$\bar{1}$) interfaces are shown in Figure 6. The rationale for their choice is explained in the final section devoted to the methodologies.

The models for the bare surface, SeCd (1 × 1), $Cd_{1/4}$/SeCd (Cd adatom), and $Se_{3/4}Cd$ (Se vacancy), Figure 6a−c, were again inspired by previous computational studies.[9,14,15] The Au thin films were obtained with subsequent steps: (1) filling the Se vacancy with Au atoms, yielding the $Au_{1/4}Se_{3/4}Cd$ structure of Figure 6d; (2) replacing the whole topmost Se plane with Au atoms, structure Au_1Cd of Figure 6e; (3) adding a full 3 × 3 Au(111) bilayer on top of the bulk-like termina-

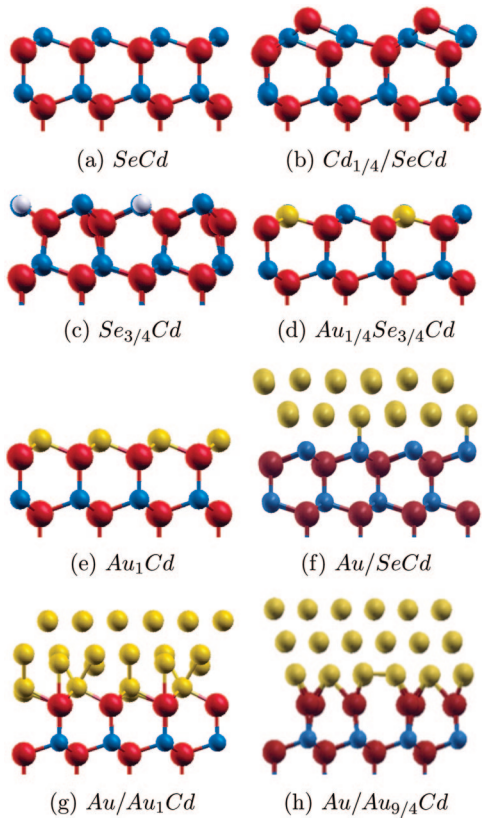

Figure 6. Side view of relaxed atomic structures for all the configurations that we examined to model the CdSe(000$\bar{1}$) surface and the Au/CdSe(000$\bar{1}$) interface. Red, blue, and yellow spheres represent Cd, Se, and Au atoms, respectively. White spheres in panel (c) represent Se vacancies.

tion of Figure 1a, which gives the structure Au/SeCd of Figure 6f; (4) adding a full 3 × 3 Au(111) bilayer on top of the surface of Figure 1e, which gives the structure Au/Au_1Cd of Figure 6g; (5) replacing the strained 2 × 2 Au interface layer of Figure 6g with a 3 × 3 Au layer while imposing the correct fcc (111) stacking through the Au thickness (structure $Au/Au_{9/4}Cd$ of Figure 6h). While for the (0001) polarity we considered only structures where Au atoms partially or fully replace the outermost Cd cations, for this (000$\bar{1}$) polarity, we consider also one structure, in Figure 6f, where there is no substitution at all of the topmost semiconductor Se layer. This is because Se atoms behave as anions, and we supposed that the exchange between overlayer metal atoms and anions could be not optimal. We also considered the structure similar $Au/Au_{1/4}Se_{3/4}Cd$ to that of Figure 1f, namely, with a 1/4 replacement by Au of the outermost semiconductor layer, but we found that it has a high formation energy with respect to Au/SeCd and do not report it here.

The calculated atomic displacements of the atoms on the three topmost bilayers are reported in Table 2, with respect to the ideal positions. As in Table 1 for the opposite polarity, the symbol * labels one out of four atoms in a plane, which behaves differently from the others, while the symbol ¯ labels the average of

TABLE 2. Calculated Vertical Atomic Displacements (in Å) at the Three Outermost Bilayers of Se- And Au-Terminated CdSe(000$\bar{1}$), Relative to the Bulk-like Positions. Positive (Negative) Values Indicate Outward (Inward) Displacements

bilayer	atom	SeCd	$Se_{3/4}Cd$	$Cd_{1/4}/SeCd$	$Au_{1/4}Se_{3/4}Cd$	Au_1Cd
1_{Se}	Se^*/Au^*			−0.15	0.18 (Au)	
	$\overline{Se}/\overline{Au}$	−0.03	−0.12	−0.05	0.04	−0.15 (Au)
1_{Cd}	Cd^*		0.11	−0.06	0.05	
	$\overline{Cd}$	−0.05	0.06	0.06	0.08	0.02
2_{Se}	Se^*		0.09	−0.03		
	$\overline{Se}$	0.01	−0.01	0.03	0.03	−0.03
2_{Cd}	$\overline{Cd}$	0.02	0.01	0.01	−0.02	0.00
3_{Se}	$\overline{Se}$	0.04	−0.01	0.02	−0.05	0.00
3_{Cd}	$\overline{Cd}$	0.02	−0.01	0.00	−0.03	0.01

equivalent atoms in a plane. The vertical displacements at our (000$\bar{1}$) structures are overall much smaller than for the (0001) structures.

Contrary to the case of the other polarity, the bulk-like terminated structure SeCd maintains the 1 × 1 symmetry even in the computational 2 × 2 supercell. All the Se atoms in the top plane are equivalent and practically at the same positions as in the bulk. This structure does not underlie any mechanisms to saturate the surface Se dangling bonds, and in fact, we see below that it has a rather high formation energy relative to the other structures, and it is metallic (though we do not show the electronic structure here). The vertical displacements in all the other tabulated layers are also negligible.[9]

In the $Se_{3/4}Cd$ surface, the three Se atoms of the top plane move slightly inward by 0.12 Å, to receive the partial charge from the three Cd dangling bonds created by the Se vacancy. Since each Cd (Se) dangling bond contains 2/4 (6/4) electrons in the tetrahedral coordination typical of the wurtzite phase; such a charge transfer is able to fill the octet in the Se atoms, giving a semiconducting structure free of surface states in the band gap.

In the $Cd_{1/4}$/SeCd surface, the three Se atoms bonded to the Cd adatom remain practically in the ideal plane (only 0.05 Å inward), while the Se^* restatom moves inward by 0.15 Å. This is compatible, again, with a charge transfer from the Cd adatom to the Se^* restatom to fill the octet and accomplish a semiconducting structure. This structure is however unfavorable relative to the Se vacancy surface independently of the Se and Cd chemical potentials and has a surface state in the bulk gap.

Tiny displacements are propagated below the outermost bilayer in all the structures. A schematic detailed side view of the relaxed atomic geometries for the CdSe(000$\bar{1}$) bare surfaces is depicted in Figure 7.

The largest bond length between the Se and Cd atoms in the first bilayer for the bare surfaces is 2.67, 2.77, and 2.59 Å for SeCd, $Cd_{1/4}$/Se, and $Se_{3/4}$, respec-

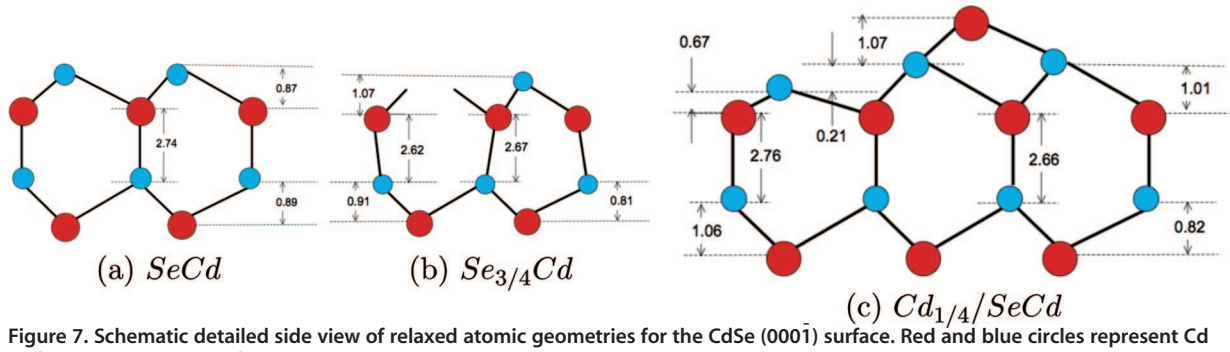

Figure 7. Schematic detailed side view of relaxed atomic geometries for the CdSe (000$\bar{1}$) surface. Red and blue circles represent Cd and Se atoms, respectively.

tively. In the second bilayer, it is, in the same order, 2.67, 2.67, and 2.68 Å. The Cd adatom is located 1.07 Å above the plane of its three Se neighbors with a corresponding Cd−Se bond length of 2.65 Å. These values are all very similar to the bulk bond length of 2.69 Å. Comparing the Cd−Se bond lengths at the (0001) and (000$\bar{1}$) surfaces, as well as the atomic displacements occurring at the reconstructed surfaces with the two opposite polarities, we note that the effect of structural optimization is more pronounced for the Cd face, namely, the (0001) polarity.

In Figure 8, we report our results about the relative energetics of the explored CdSe(000$\bar{1}$) surfaces and Au/CdSe(000$\bar{1}$) interfaces as a function of the chemical potentials of the different constituting species. The different panels are obtained from eq 2 as explained for Figure 3. Differently from the plots in Figure 3a,b, we plot the relative formation energies of the various structures for the Se face against the Se chemical potential using in eq 2 the relation $\mu_{Cd} = \mu_{Se} - \Delta H_{CdSe}$ because the stoichiometry at this face is rather controlled by the Se abundance. This means that Cd-rich and Se-rich conditions are exchanged from left to right relative to Figure 3. Plotting against μ_{Cd} would just mean inverting the slope of all curves and is automatically done by reading the plots from right to left.

The plot of Figure 8a shows that in extremely Au-rich conditions, fixed by $\mu_{Au} = \mu_{Au(bulk)}$, the lowest energy structure among those considered by us includes a thin Au film on top of the CdSe substrate. This means that also on this polarity epitaxial deposition is feasible at the very beginning in suitable Au abundance.

By decreasing the Au abundance, all the structures containing Au atoms are raised in energy because of the strain energy cost. In the case $\mu_{Au} = \mu_{Au(bulk)} - 0.25$ eV illustrated in Figure 8b, for instance, the $Au/Au_{9/4}Cd$ is still favorable over most of the allowed range of μ_{Se}, except in Se-rich ambient where the Au/SeCd surface, which requires no Se removal, is preferred. By further decreasing the Au chemical potential, we find that no thin films or mixed interfaces are energetically favorable, independently of the Se stoichiometry, for $\mu_{Au} \leq \mu_{Au(bulk)} - 0.40$ eV, where the bare $Se_{3/4}Cd$ surface is preferred.

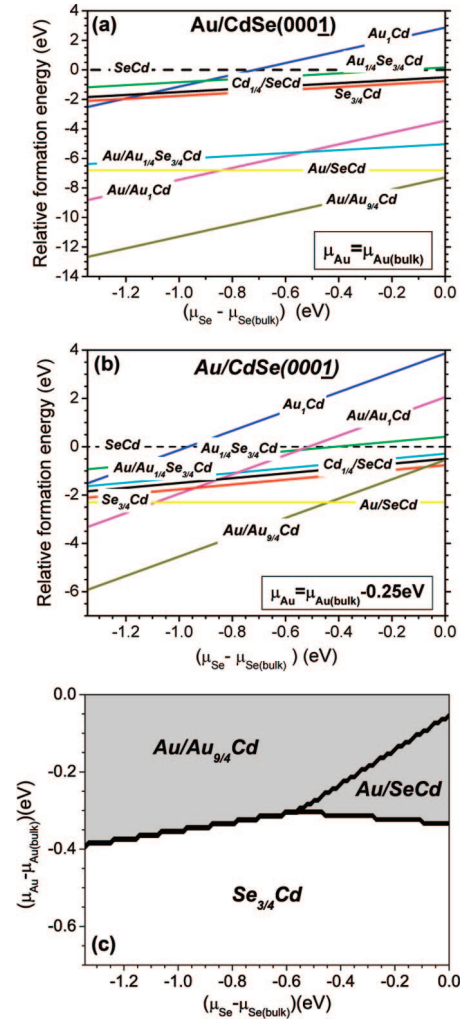

Figure 8. (a) Relative formation energy, computed with respect to the arbitrary reference SeCd surface, as a function of the Se chemical potential for a fixed Au abundance equal to that of bulk fcc Au (Au-rich conditions). (b) Relative formation energy, computed with respect to the arbitrary reference SeCd surface, as a function of the Se chemical potential for a fixed Au abundance lower than that of bulk fcc Au. (a,b) Cd-rich (Se-rich) conditions mark the lower (upper) limit of the horizontal axis. (c) Phase diagram representing the lowest energy structure in the plane of variability of both μ_{Au} and μ_{Cd}. The upper limit of μ_{Au} corresponds to Au-rich conditions, fixed at bulk fcc Au, and an arbitrary lower limit is chosen. The upper (lower) limit of μ_{Se} corresponds to a Se-rich (Se-poor equivalent to Cd-rich), fixed at hexagonal bulk Se, CdSe surface with respect to the stoichiometric bulk: the lower limit is fixed by the formation energy of bulk CdSe (see Theoretical Framework).

By looking at the summarizing stability diagram of Figure 8c, we point out that only the above three structures play a role. The stability of the bare $Se_{3/4}Cd$ surface over a wide range of stoichiometries reflects the fact that this reconstruction fulfills the electron counting rule by allowing for emptying the cation dangling bonds and filling the anion dangling bonds, as we commented above in relation to the structural features and will see more specifically below in the electronic structure.

The situation is overall very similar to that found for the (0001) polarity, namely, thin epitaxial Au films need rather Au-rich conditions to be stabilized on top of the CdSe substrate. In addition, the situation in terms of μ_{Cd} and μ_{Se} must be compatible with the removal of substrate atoms from the top plane for gradual substitution with Au.

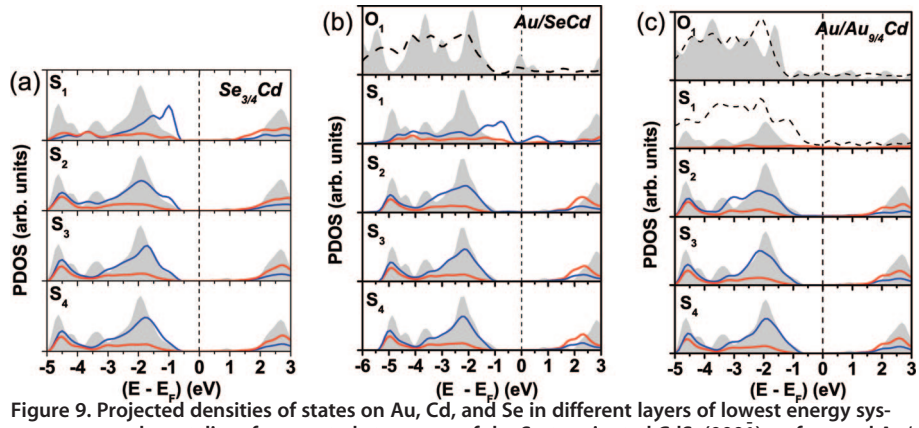

Figure 9. Projected densities of states on Au, Cd, and Se in different layers of lowest energy systems among the totality of computed structures of the Se-terminated CdSe(000$\bar{1}$) surface and Au/CdSe(000$\bar{1}$) interfaces, namely, those that appear in the phase diagram of Figure 8. The labels of the structures conform to the definitions in Figure 6. S_1, S_2, S_3, and S_4 indicate the four topmost substrate bilayers, and O_1 indicates the Au overlayer on top of the S_1 bilayer. The S_1 bilayer is purely SeCd in $Se_{3/4}Cd$ and in Au/SeCd, while the Cd layer is mixed with Au atoms in $Au/Au_{9/4}Cd$. The shaded gray area is the CdSe-wurtzite bulk DOS in the panels for substrate bilayers and is the Au fcc bulk DOS in the panels for the overlayer. The solid red and blue lines indicate the contributions of the Cd and Se states, respectively. The dashed black lines indicate the contributions of the Au states. The vertical lines denote the positions of the Fermi energy. The bottom of the valence band from interface calculations is aligned to the bottom of the valence band of wurtzite bulk CdSe. Layer S_4 is representative of the bulk features.

CdSe (000 $\bar{1}$) and Au/CdSe (000 $\bar{1}$): Electronic Properties. In Figures 9 and 10, we plot the layer-projected DOS and the bandstructure, respectively, for the lowest energy CdSe(000$\bar{1}$) surfaces and Au/CdSe(000$\bar{1}$) interfaces that appear in the stability diagram of Figure 8c.

Having already identified the general electronic features of the bulk phases and the electronic mechanisms active at high-energy conformations in the context of the other polarity, we directly comment here just the structures included in Figure 9, representative of the low-energy phases.

For the $Se_{3/4}Cd$ surface, the plot in Figure 9a is consistent with the reconstruction mechanism suggested in the previous subsection. The structure has a band gap that is essentially equal to the bulk band gap because as a consequence of the atomic displacements the Cd dangling bonds can transfer electrons to the Se dangling bonds, so that there are no partially occupied bands. The edge of the Se PDOS, however, is different than in the bulk because of a reorientation of the dangling bonds from a direction perpendicular to the surface to a more oblique direction (see Figure 10a). This is slightly different from what happens in the case of the Cd vacancy surface ($Cd_{3/4}Se$) of the opposite polarity, where instead there are no Se dangling bonds originally perpendicular to the surface but all toward the bulk.

The structures Au/SeCd and $Au/Au_{9/4}Cd$ containing a Au overlayer are metallic, as shown in Figures 9b,c and 10b,c. However, at this Se face, we do not find a significant metal−semiconductor electronic hybridization for the structure $Au/Au_{9/4}Cd$ that includes metal−semiconductor atomic exchange. At the $Au/Au_{9/4}Cd$ interface, the first available Se atoms to hybridize with Au are on the S_2 bilayer (see orbital in Figure 10c, top inset). There is a slight mixing of Au orbitals with Cd-localized orbitals, but this is not favorable in terms of electronegativity, and in fact, the resulting DOS at the Fermi level is almost vanishing (see S_1-PDOS in Figure 9d). Most of the bands that cross the Fermi level are instead due to electron states localized in the metal film (see Figure 10b). We find instead a slight Au−Se hybridization around the Fermi level for the Au/SeCd interface; in fact, the Se-PDOS at S_1 in Figure 9b has a small component at the Fermi level, where the Au-PDOS at O_1 is peaked, and the wave functions of Figure 10b show mixed Se−Cd character.

FINAL REMARKS

In summary, we have reported *ab initio* calculations of the polar (0001) and (000$\bar{1}$) Au/CdSe interfaces. The atomic interface geometries have been calculated by total energy minimization in the DFT framework using plane waves and pseudopotentials.

On the basis of the results presented and discussed above, we can draw the following general features.

(i) The bare surfaces with Cd or Se vacancies, at the (0001) and (000$\bar{1}$) surfaces, respectively, are stable against the deposition of Au films in a wide range of atomic chemical potentials.

(ii) Stable Au bilayers may be formed on the CdSe surfaces within the allowed range of Cd/Se chemical potential and in Au-rich conditions, at both polarities. This is in line with the fact that Au nanoparticles are grown to decorate CdSe nanorods at both edges of the rods, which have by construction opposite polarities.[4,5]

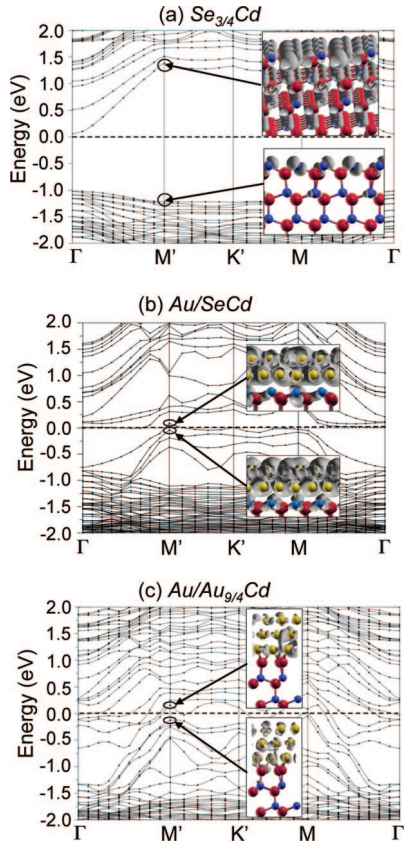

Figure 10. Band structure for the low-energy CdSe(000$\bar{1}$) and Au/CdSe(000$\bar{1}$) interfaces that are relevant in the stability diagram of Figure 8. The horizontal dashed lines denote the positions of the Fermi level, set at the origin of the energy scale. The insets represent electron states at the M′ point around the band gap of semiconducting structures or the Fermi level of metallic structures.

We remark, however, that the thin films investigated by us cannot be extended epitaxially to nanometer size because of the strain energy that must be released beyond a certain critical thickness. Yet, we believe that the interface electronic features are representative of real cases of nanodumbbells. This latest statement is also supported by the fact that all the interfaces considered by us, independently of the precise interface stoichiometry, behave very similarly from the electronic point of view: the metallic behavior is confined at the overlayer and at the very interface plane, with quantitative differences but qualitative equivalence.

(iii) Atomic mixing between the semiconductor and the metal is predicted in the topmost substrate bilayer: in fact, all the low-energy Au thin films contain a mixed Cd−Au (000$\bar{1}$) or Se−Au (0001) interface bilayer. However, atomic mixing is not favorable in a single plane.

(iv) All the thin films that we have considered and that turn out to be favorable in some areas of the stability diagrams are metallic, as dictated by the presence of the Au overlayer. However, local probes to characterize the properties of metal−semiconductor nanodumbbells should in principle be able to distinguish the semiconducting from the metal component of the nanostructure, as inferred from the separation of the PDOS components into the layers of the structures: from the second bilayer inward, none of the low-energy structures has a finite DOS at the Fermi level, and none has a Au contribution in the layer-projected PDOS.[4,6−8]

(v) The natural intuition is that, for the creation of a smooth epitaxial interface, Au is likely to replace the cationic character of Cd but less prone to replace the anionic character of Se. As a consequence, we find indeed that Se−Au hybridization is significant at the (0001) face because Au replaces Cd forming bonds with Se. On the other hand, Au−CdSe hybridization is almost negligible at the (000$\bar{1}$) face because none of the possible configurations is compatible with bonding: the plane adjacent to Au is in fact a Cd plane, and the Cd states are less reactive than the Se states because they lie in a lower energy range (as we said above, the top of the valence band has the fingerprint of Se p states).

(vi) Even in the cases where there is efficient interface hybridization, the interface mixed orbitals are confined at the interface layer. This is encouraging for the development of model theoretical approaches that can treat realistic nanoparticle sizes for the investigation of the optical properties without taking into account the coupling between the metal and the semiconductor due to electronic interactions, but still retaining the coupling due to electrostatics and screening. In fact, the account for electronic interactions would be beyond any possibility of upgrade of currently available methods to compute the scattering response of metal nanoparticles. Such available methods are for instance classical approaches such as, for example, the discrete dipole approximation (DDA)[16] in which the continuum space is replaced by a number of dipoles on a discrete grid that respond to the excitation field and the similar boundary element method,[17] but there are also quantum methods that describe the excitonic response of semiconductors in terms of a configuration interaction scheme on top of the envelope-function ground-state treatment.[18,19] On the contrary, both classes of methods can be extended to take into account the presence of a dielectric environment that modifies both the plasmonic response of the metal and the excitonic response of the semiconductor.

THEORETICAL FRAMEWORK

***Ab Initio* Simulations.** We carried out self-consistent first-principle calculations using the plane-wave pseudopotential method within the density functional formalism as implemented in the PWSCF code.[20] We used ultrasoft pseudopotentials to treat the interaction between the atomic cores and the valence

electrons and the PBE generalized gradient approximation for the exchange-correlation potential.[21,22] The Cd 4d and Au 5d electrons were included as valence electrons. The Se 3d electrons were frozen in the atomic core and treated with nonlinear core corrections.

The plane-wave kinetic energy cutoff and the Brillouin zone sampling grid for our surface calculations were chosen on the basis of bulk tests. For wurtzite CdSe at the experimental lattice constants, using the above ingredients in single-point self-consistent calculations, we varied the plane-wave kinetic energy cutoff between 20 and 45 Ry and sampled $2 \times 2 \times 1$, $4 \times 4 \times 2$, and $8 \times 8 \times 4$ Monkhorst-Pack meshes[23] for each cutoff. We found that the total energy and the electronic band gap were converged with 25 Ry and the $4 \times 4 \times 2$ mesh. With this chosen convergence parameters, we then relaxed the lattice constants a and c/a of wurtzite CdSe to check the performance of our method against experimental values and to determine the theoretical lattice constants that we adopted in the surface and interface calculations. The calculated parameters of wurtzite bulk CdSe are found to be $a = 4.365$ Å, $c/a = 1.645$, $u = 0.375$, yielding a Cd−Se bulk bond length of 2.69 Å, in good agreement with previous experimental and theoretical studies.[9,14,15,24−27]

For the surface and interface calculations, we employed the periodically repeated supercell approach, by which the two-dimensional (2D) systems are described by repeated slabs that contain few atomic layers sufficient to describe the bulk and the surfaces and a vacuum thickness that ensures negligible spurious interactions between neighboring replicas. To fix the lateral extent of the supercells, we started from the consideration that the 3×3 Au(111) hexagonal lattice is almost commensurate to the 2×2 CdSe(0001) hexagonal lattice, with a 0.6% strain.[28] Thus we used supercells with a 2D lattice equivalent to the 2×2 lattice of the CdSe substrate. Consequently, we adopted a $2 \times 2 \times 1$ Monkhorst-Pack mesh consistent with the $4 \times 4 \times 2$ convergence mesh for the bulk. The simulation supercells included eight CdSe bilayers and a vacuum region 16 Å thick. The Cd or Se atoms of the top surface plane, in the (0001) or (000$\bar{1}$) polarity, respectively, were partially (1/4) or fully (4/4 and 9/4) replaced by Au atoms. We further considered the addition of two Au(111) 3×3 layers on top of the initial interfaces. The bottom side of the slab was saturated with pseudo-hydrogen atoms of fractional charge 0.5 e^- to saturate the bottom Se dangling bonds of the CdSe(0001) surface and 1.5 e^- to saturate the bottom Cd dangling bonds of the CdSe(000$\bar{1}$) surface. This dangling bond saturation is a standard computational artifact to ensure unphysical charge transfer between the two ends of the slab and avoids the appearance of spurious surface states in the gap.[9,29,30] Starting from guess structures guided by the electron counting rule, each atomic configuration was fully relaxed until all atomic forces were smaller than 0.02 eV/Å (Figures 1 and 2).[29−31] Although the clean surfaces were already investigated in the recent past at a comparable DFT level, we need to include them in our study because we wish to unravel under which conditions Au thin films may coexist on the substrate, and to this aim we need to calculate the total energies of all the structures consistently with the same computational details.[9,14,15]

The definition of the total density of states of a given system is $\mathrm{DOS}(E) = \sum_{i,k} |\langle\psi_{ik}|\psi_{ik}\rangle|^2 \delta(E - \epsilon_{ik})$, where ψ_{ik} and ϵ_{ik} are the eigenfunctions and eigenvalues of the DFT Kohn−Sham equations, namely, the single-particle wave functions and electronic levels of the whole system, i is the band index and k is the reciprocal-space index. The projected density of states on a given atomic orbital or set of atomic orbitals is a measure of how much of the DOS reveals the contribution of that (set of) orbital(s). For instance, the PDOS on all the atomic orbitals of a given species indicates in which energy regions the orbitals of that species appear. It is obtained by projecting the wave functions of the total system (Kohn−Sham eigenfunctions) onto individual atomic orbitals of the chosen species and then summing over all orbitals of interest: $\mathrm{PDOS}_s(E) = \sum_j \sum_{i,k} |\langle\Phi_j^s|\psi_{ik}\rangle|^2 \delta(E - \epsilon_{ik})$, where s is the species index and j is the orbital index for species s, i, and k have the same meaning as above. In our case, $j = 1$ for s orbitals, $j = 1-3$ for p orbitals, and $j = 1-5$ for d orbitals. To obtain the Se-PDOS, we sum over s and p orbitals, namely, over four orbitals. To obtain the Cd-PDOS and Au-PDOS, we sum over s, p, and d orbitals, namely, over nine orbitals.

For the alignment of the interface DOS to the bulk DOS in Figures 4 and 9, we have chosen the method that exploits the bottom the valence band, as an alternative to the alignment of the macroscopic-averaged potential. The validity of our approach is subjected to the condition that the bottom of the valence band has a bulk character and does not depend on the slab thickness. If this is true, then the two methods are equivalent. We have indeed verified that the electronic level that we use for band alignment is a bulk. We are also confident that the slab thickness is sufficiently large because, as we comment about Figures 4 and 9, we already have a bulk-like behavior on bilayers 3 and 4, which means a total of six bulk bilayers, given the fact that the pseudo-H-saturated bottom surface is practically bulk-like.

Treatment of the Relative Energetics. To compare the formation energies of structures that contain different numbers of atoms of the various species, the total energy is not the quantity of choice. We thus follow a zero-temperature thermodynamics approach that takes into account the chemical potentials of the constituent species.[29,30,32] The chemical potentials may vary depending on the preparation conditions.

The general expression of the formation energy (E_f) depends on the number of atoms of the various species. Here we analyze separately the (0001) and (000$\bar{1}$) polarities, at odds with what was done by other authors following a recently proposed scheme to compute the absolute formation energy of polar surfaces.[9,14,15,33] We do so because our interest is focused on analyzing the formation of Au overlayers at each polarity and the possible consequent electronic hybridization, rather than comparing the formation energies of different facets to shed light on the growth modes of the nanorods. By separating the two polarities, we simplify the problem by calculating formation energy differences (rather than absolute values) and avoiding the treatment of the H-passivated surfaces; in fact, all the systems with a given polarity have the same bottom surface, and the energy differences do not depend on the number of the pseudo-H atoms.[33] The relative formation energy ΔE_f of any given structure with respect to an arbitrarily chosen reference structure is

$$\Delta E_f = \Delta E_{tot} - \Delta n_{Au}\mu_{Au} - \Delta n_{Cd}\mu_{Cd} - \Delta n_{Se}\mu_{Se} \quad (1)$$

ΔE_{tot} is the total-energy difference between a given structure and the reference system; μ_i is the chemical potential of the atomic species i; Δn_i is the difference between the number of atoms of species i in a given structure and the number of atoms of species i in the reference configuration. We can assume the condition that the surfaces and interfaces under study are in equilibrium with the bulk substrate, so that $\mu_{Cd} + \mu_{Se} = \mu_{CdSe(bulk)}$, where $\mu_{CdSe(bulk)}$ is the total energy per CdSe pair of wurtzite bulk CdSe. This constraint reduces the number of independent variables in eq 1. By expressing μ_{Se} as a function of μ_{Cd}, the latter remains explicitly in eq 1 and may vary in the range $\mu_{Cd(bulk)} - \Delta H_{CdSe} < \mu_{Cd} < \mu_{Cd(bulk)}$, where the upper (lower) limit corresponds to Cd-rich (Se-rich) conditions and ΔH_{CdSe} is the heat of formation of wurtzite CdSe. The computed heat of formation is 1.34 eV, in agreement with other theoretical results.[9]

With a few algebraic steps, eq 1 can be recast as

$$\Delta E_f = [\Delta E_{tot} - \Delta n_{Se}\mu_{CdSe(bulk)}] - [\Delta n_{Cd} - \Delta n_{Se}]\mu_{Cd} - \Delta n_{Au}\mu_{Au} \quad (2)$$

The first term is a constant for any given structure: a bulk calculation to determine μ_{CdSe} is needed once for all the series of analyzed surface/interface configurations. Two more small bulk calculations are needed to comparatively analyze the whole series of interface structures, namely, those for the bulk phases of hcp Cd (2 atoms/cell, D_{6h}^4 space group) and hexagonal Se (3 atoms/cell, D_3^4 space group) to evaluate the term ΔH_{CdSe} that fixes the allowed range of μ_{Cd} and μ_{Se}.

In the case of clean substrate surfaces, $\Delta n_{Au} = 0$, and the relative formation energy has a linear dependence on the Cd chemical potential only. ΔE_f can be plotted against μ_{Cd}, and the

most favorable structure for any value of μ_{Cd} is simply determined as the structure of minimum ΔE_f for that μ_{Cd}. However, in the case of Au-covered CdSe surfaces, eq 2 depends on two independent variables, and one must find an alternative way to present the results. We identify different possibilities. (1) One can assume fixed Au abundance conditions, which is equivalent to fixing the Au chemical potential. (2) One can explore the stability diagram as a function of both μ_{Cd} and μ_{Au}, by plotting maps that identify the minimum energy structures in the $[\mu_{Cd},\mu_{Au}]$ plane. Below, we present results in both ways. For the former case, we choose Au-rich conditions $\mu_{Au} = \mu_{Au(bulk)}$ and an arbitrary and nonrestictive condition of less abundance $\mu_{Au} = \mu_{Au(bulk)} - 0.25$ eV. For the latter case, while the range of variability of μ_{Cd} is naturally fixed by the heat of formation of CdSe bulk, there is no natural condition to fix the Au chemical potential in the present problem, unless one considers the temperature dependence; hence, we choose a variability range of 0.7 eV for μ_{Au}. Despite this range is somewhat arbitrary, we believe it does not affect our results because, as we discuss later, the Au-ordered layers become relevant only for rather high values of μ_{Au}, close to the Au-rich conditions.

Acknowledgment. This work was supported, within the EU FP6, by the ERANET project NanoSci-ERA: NanoScience in the European Research Area. We acknowledge fruitful discussions with Fabrice Vallee, Natalia Del Fatti, Guido Goldoni, Uri Banin, and Carsten Sönnichsen within the project NanoSci-ERA subproject "Single Nano-Hybrid". Computer time was granted by INFM-CNR at the CINECA supercomputers through the Parallel Computing Initiative.

REFERENCES AND NOTES

1. Lee, K.-S.; El Sayed, M. A. Gold and Silver Nanoparticles in Sensing and Imaging: Sensitivity of Plasmon Response to Size, Shape, and Metal Composition. *J. Phys. Chem. B* **2006**, *110*, 19220–19225.
2. Lee, J.; Hernandez, P.; Lee, J.; Govorov, A. O.; Kotov, N. A. Exciton-Plasmon Interactions in Molecular Spring Assemblies of Nanowires and Wavelength-Based Protein Detection. *Nat. Mater.* **2007**, *6*, 291–295.
3. Kan, S.; Mokari, T.; Banin, U. Synthesis and Size-Dependent Properties of Zinc-Blende Semiconductor Quantum Rods. *Nat. Mater.* **2003**, *2*, 155–158.
4. Mokari, T.; Rothenberg, E.; Popov, I.; Costi, R.; Banin, U. Selective Growth of Metal Tips onto Semiconductor Quantum Rods and Tetrapods. *Science* **2004**, *304*, 1787–1790.
5. Mokari, T.; Sztrum, C. G.; Salant, A.; Rabani, E.; Banin, U. Formation of Asymmetric One-Sided Metal-Tipped Semiconductor Nanocrystal Dots and Rods. *Nat. Mater.* **2005**, *4*, 855–863.
6. Saunders, A. E.; Popov, I.; Banin, U. Synthesis of Hybrid CdS-Au Colloidal Nanostructures. *J. Phys. Chem. B* **2006**, *110*, 25421–25429.
7. Steiner, D.; Mokari, T.; Banin, U.; Millo, O. Electronic Structure of Metal-Semiconductor Nanojunctions in Gold CdSe Nanodumbbells. *Phys. Rev. Lett.* **2005**, *95*, 056805−1056805−4.
8. Rothenberg, E.; Kazes, M.; Shaviv, E.; Banin, U. Electric Field Induced Switching of the Fluorescence of Single Semiconductor Quantum Rods. *Nano Lett.* **2005**, *5*, 1581–1586.
9. Manna, L.; Wang, L. W.; Cingolani, R.; Alivisatos, A. P. First-Principles Modeling of Unpassivated and Surfactant-Passivated Bulk Facets of Wurtzite CdSe: A Model System for Studying the Anisotropic Growth of CdSe Nanocrystals. *J. Phys. Chem. B* **2005**, *109*, 6183–6192.
10. Puzder, A.; Williamson, A. J.; Zaitseva, N.; Galli, G.; Manna, L.; Alivisatos, A. P. The Effect of Organic Ligand Binding on the Growth of CdSe Nanoparticles Probed by *Ab Initio* Calculations. *Nano Lett.* **2004**, *4*, 2361–2365.
11. Puzder, A.; Williamson, A.; Gygi, F.; Galli, G. Self-Healing of CdSe Nanocrystals: First-Principles Calculations. *Phys. Rev. Lett.* **2004**, *92*, 217401-1–217401-4.
12. Rabani, E. Structure and Electrostatic Properties of Passivated CdSe Nanocrystals. *J. Chem. Phys.* **2001**, *115*, 1493–1497.
13. Wangnt, L. G.; Pennycook, S. J.; Pantelides, T. S. The Role of the Nanoscale in Surface Reactions: CO_2 on CdSe. *Phys. Rev. Lett.* **2002**, *89*, 075506-1–075506-4.
14. Rempel, J. Y.; Trout, B. L.; Bawendi, M. G.; Jensen, K. F. Properties of the CdSe(0001), (000$\bar{1}$), and (11$\bar{2}$0) Single Crystal Surfaces: Relaxation, Reconstruction, and Adatom and Admolecule Adsorption. *J. Phys. Chem. B* **2005**, *109*, 19320–19328.
15. Rempel, J. Y.; Trout, B. L.; Bawendi, M. G.; Jensen, K. F. Density Functional Theory Study of Ligand Binding on CdSe (0001), (000$\bar{1}$), and (11$\bar{2}$0) Single Crystal Relaxed and Reconstructed Surfaces: Implications for Nanocrystalline Growth. *J. Phys. Chem. B* **2006**, *110*, 18007–18016.
16. Draine, B. T.; Flatau, P. J. Discrete-Dipole Approximation for Scattering Calculations. *J. Opt. Soc. Am. A* **1994**, *11*, 1491–1499; http://www.astro.princeton.edu/~draine/DDSCAT.6.0.html.
17. Trügler, A.; Hohenester, U. Strong Coupling Between a Metallic Nanoparticle and a Single Molecule. *Phys. Rev. B* **2008**, *77*, 115403-1–115403-6.
18. Rontani, M.; Cavazzoni, C.; Bellucci, D.; Goldoni, G. Full Configuration Interaction Approach to the Few-Electron Problem in Artificial Atoms. *J. Chem. Phys.* **2006**, *124*, 124102-1–124102-14.
19. Hohenester, U. *Ab-Initio* Calculation of Optical Absorption in Semiconductors: A Density-Matrix Description. *Phys. Rev. B* **2001**, *64*, 205305-1–205305-9.
20. Baroni, S.; Corso, A. D.; de Gironcoli, S.; Giannozzi, P.; Cavazzoni, C.; Ballabio, G.; Scandolo, S.; Chiarotti, G.; Focher, P.; Pasquarello, A. *et al.* PWSCF and PHONON: Plane-Wave Pseudo-Potential Codes, version 3.2; http://www.pwscf.org, 2007.
21. Vanderbilt, D. Soft Self-Consistent Pseudopotentials in a Generalized Eigenvalue Formalism. *Phys. Rev. B* **1990**, *41*, 7892–7895.
22. Perdew, J. P.; Burke, K.; Ernzerhof, M. Generalized Gradient Approximation Made Simple. *Phys. Rev. Lett.* **1996**, *77*, 3865–3868.
23. Monkhorst, H. J.; Pack, J. D. Special Points for Brillouin-Zone Integrations. *Phys. Rev. B* **1976**, *13*, 5188–5192.
24. Parthasarathy, G.; Holzapfel, W. B. Structural Phase Transitions and Equations of State for Selenium under Pressure. *Phys. Rev. B* **1988**, *38*, 10105–10108.
25. Yeh, C.-Y.; Lu, Z. W.; Froyen, S.; Zunger, A. Zinc-Blende-Wurtzite Polytypism in Semiconductors. *Phys. Rev. B* **1992**, *46*, 10086–10097.
26. *CRC Handbook of Chemistry and Physics* a ready-reference book of chemical and physical data; Lide, D. R., Ed.; CRC Press: New York, 1996; pp 9−53.
27. Jette, E. R.; Foote, F. Precision Determination of Lattice Constants. *J. Chem. Phys.* **1935**, *3*, 605–616.
28. Lister, T. E.; Stickney, J. L. Formation of the First Monolayer of CdSe on Au(111) by Electrochemical ALE. *Appl. Surf. Sci.* **1996**, *107*, 153–160.
29. Di Felice, R.; Northrup, J. E.; Neugebauer, J. Energetics of AlN Thin Films and the Implications for Epitaxial Growth on SiC. *Phys. Rev. B* **1996**, *54*, R17351−R17354.
30. Northrup, J. E.; Di Felice, R.; Neugebauer, J. Atomic Structure and Stability of AlN(0001) and (000$\bar{1}$) Surfaces. *Phys. Rev. B* **1997**, *55*, 13878–13883.
31. Srivastava, G. P. The Electron Counting Rule and Passivation of Compound Semiconductor Surfaces. *Appl. Surf. Sci.* **2006**, *252*, 7600–7607.
32. Qian, G.-X.; Martin, R. M.; Chadi, D. J. First-Principles Study of the Atomic Reconstructions and Energies of Ga- and As-Stabilized GaAs(100) Surfaces. *Phys. Rev. B* **1998**, *38*, 7649–7663.
33. Zhang, S. B.; Wei, S.-H. Surface Energy and the Common Dangling Bond Rule for Semiconductors. *Phys. Rev. Lett.* **2004**, *92*, 086102-1–086102-4.